Astron. Astrophys. 356, L83–L87 (2000)

ASTRONOMY AND ASTROPHYSICS

LETTER

Letter to the Editor

The cold dust concentrations in the colliding galaxies NGC 4038/39⋆

M. Haas[1], **U. Klaas**[1], **I. Coulson**[2], **E. Thommes**[1,3], **and C. Xu**[4]

[1] Max–Planck–Institut für Astronomie (MPIA), Königstuhl 17, 69117 Heidelberg, Germany
[2] Joint Astronomy Centre, 660 N. Aohuku Place, University Park, Hilo 96720, Hawaii, USA
[3] Royal Observatory, Blackford Hill, Edinburgh EH9 3HJ, UK
[4] Infrared Processing and Analysis Center, Jet Propulsion Laboratory, Caltech 100-22, Pasadena, CA91125, USA

Received 3 March 2000/ Accepted 18 March 2000

Abstract. SCUBA 450 and 850 μm maps of the Antennae Galaxy resolve the nuclei of NGC 4038/39 and two prominent regions in the overlap area of the galaxy disks. They coincide excellently with bright emission peaks seen on 15 μm, 6 cm and CO maps. ISOPHOT 60 and 100 μm maps reveal that the overlap area and the NGC 4038 nucleus are also responsible for the bulk of the far-infrared emission. In addition to the prominent emission from dust at a temperature of about 30 K, typical for active starburst galaxies, cold dust at temperatures below 20 K is found like in quiescent galaxies and dense cloud complexes. Thus, the observations suggest a common phenomenon for merging galaxies: besides the warm dust heated by active starbursts they possess simultaneously dense concentrations of cold dust which are presumably in a pre-starburst phase. The dust mass in the two overlap region knots is about 10^7 $M_\odot$ which comprises a considerable fraction of the typical dust content of a whole spiral galaxy. Such a high concentration could be explained by an initial inelastic collision of clouds which loose their angular momentum and serve as concentrating kernels into which the other clouds rotating in the disks are running. The two submm knots seem to comprise independent kernels, since they are too far separated to be mutually triggered.

Key words: galaxies: fundamental parameters – galaxies: individual: – galaxies: interactions – galaxies: photometry – infrared: galaxies

1. Introduction

NGC 4038/39 (Arp 244, distance 21 Mpc) is the prototype of an interacting system with spectacular tidal tails, "The Antennae". While the stars in such interacting systems undergo *elastic* collisions and the resulting shape is best outlined in the optical (e.g. the HST image in Whitmore & Schweizer 1995), the interstellar matter suffers *inelastic* collisons. Hence, it will be differently distributed than the stars. Also, bursts of star formation occur: Tidal forces shock and compress the gas so that it finally collapses into new stars. Exceptional star formation knots have been observed in the overlap region between the two nuclei of NGC 4038/39 with ISOCAM at 7-15 μm, sensitive to warm dust (Mirabel et al. 1998). The brightest knot which even outshines both nuclei, is inconspicuous at optical wavelengths. The HST image rather shows a pronounced dust lane between the two reddened nuclei. Thus, the starbursts are hidden behind enormous amounts of dust.

Based on 10-200 μm ISO photometry the luminosity of warm and cold dust emission has been determined for the total galaxy ($6.4 \cdot 10^{10}$ $L_\odot$, Klaas et al. 1997), and Kuiper Airbourne Observatory 100 and 160 μm maps, though with limited spatial resolution, suggest a major contribution from the overlap region (Bushouse et al. 1998). Here, we resolve the distribution of the cold dust ($T < 40$ K) showing up between 60 and 850 μm using SCUBA (Holland et al. 1999) at the JCMT and ISOPHOT (Lemke et al. 1996) onboard ISO (Kessler et al. 1996). The dust serves as an excellent tracer of interstellar matter. Its luminosity and temperature provide clues to heating processes and evolutionary states: Of particular interest in this early stage of merging galaxies is, how far heating by starbursts has already onset or whether dust cloud complexes are still in a pre-starburst phase.

2. Observations and data reduction

SCUBA: Jiggle maps at 450 and 850 μm with 15″ FWHM spatial resolution were obtained on July 3rd, 1999, under excellent and stable conditions ($\tau_{850\,\mu m} = 0.209 \pm 0.003$). The observing time was 22 min. The atmospheric transmission was determined from sky dips, and Mars and Uranus served as standard calibrators. The data were reduced using the SCUBA User Reduction Facility (SURF) including identification of noisy bolometer pixels and removal of sky noise.

ISOPHOT: The 60 and 100 μm data were retrieved from the ISO Data Archive and reduced from raw data level using the ISOPHOT Interactive Analysis tool (PIA V7.3). With a detector pixel size of 46″ and oversampling in steps of 15″ × 23″ the

Send offprint requests to: M. Haas (haas@mpia-hd.mpg.de)

⋆ Based on observations at the James Clerk Maxwell Telescope JCMT and with the Infrared Space Observatory ISO.

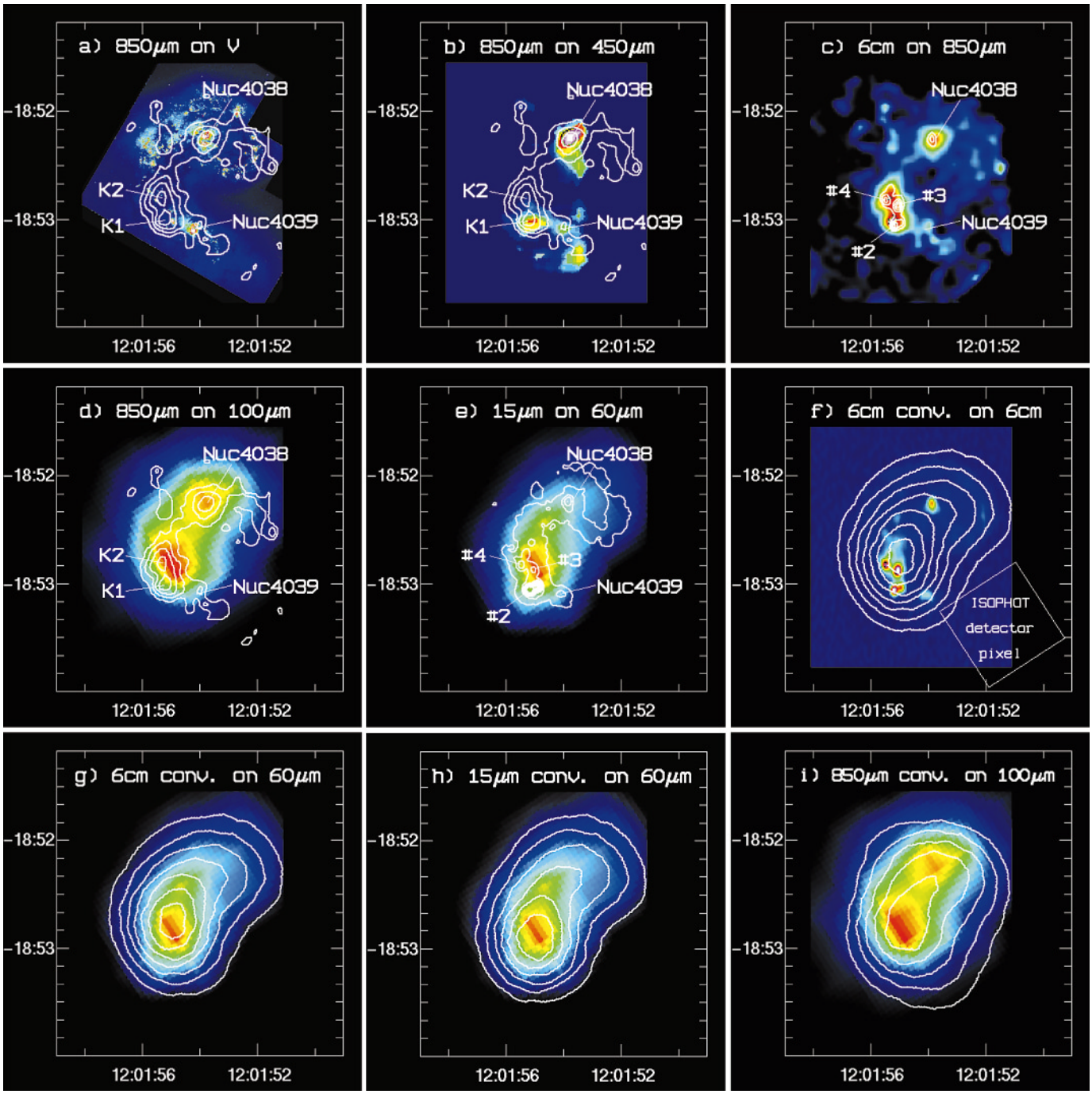

Fig. 1. a–e observed maps, and **f–i** comparison with simulated images:
a 850 μm contours on HST V image (from Whitmore & Schweizer 1995), **b** 450 μm with 850 μm contours. The 450 μm map is smoothed from about 5″ to 15″ FWHM to reduce noise. **c** 850 μm with 6 cm radio contours (from Hummel & van der Hulst 1986). The radio peaks are enumerated as in Hummel & van der Hulst and indicated with #. The brightest radio peaks #3 and #4 (in particular at 20 cm) lie at the location of K2, while #2 lies at K1. **d** 100 μm with 850 μm contours. **e** 60 μm with 15 μm contours (from Mirabel et al. 1998). The 15 μm peaks coincide spatially with those at 6 cm, with #2 being by far the brightest at 15 μm. The ISOPHOT 60 and 100 μm maps are interpolated to 1″ pixel size for better visualisation.
The offset between the FIR maxima in the overlap region and the 850 μm and 15 μm knots seen in **d** and **e** is due to the convolution of the asymmetric brightness distribution with the coarse ISOPHOT detector pixels as shown in the simulated images **f–i**. These images illustrate that during the ISOPHOT observing and mapping procedure the maximum intensity is shifted towards northwest, for details see text.
f 6 cm original map with simulation as contours: the maximum of the simulated map is shifted towards northwest, for comparison also the size and orientation of the ISOPHOT detector pixel is drawn; **g** 60 μm observed map with simulation from 6 cm as contours: good coincidence, with simulated peak lying marginally north of observed peak; **h** 60 μm observed map with simulation from 15 μm as contours: good coincidence, much better than in Fig. 1e, with simulated peak lying marginally south of observed peak; **i** 100 μm observed map with simulation from 850 μm as contours: good coincidence at the maximum in the overlap area, much better than in Fig. 1d.

maps reach a spatial resolution of about 30″ FWHM. Astrometry has to be considered with care, as the separation of point sources closer than the detector pixel size can be affected.

3. Results

Maps: The SCUBA and ISOPHOT maps are shown in Fig. 1 together with maps at other wavelengths for comparison.

On the SCUBA maps (Fig. 1a-c) the most striking features are the two equally bright 850 μm emission knots in the image centre (henceforth called K1 and K2). They are located in the overlap region of the two galaxy disks. At 850 μm the northern nucleus NGC 4038 is also prominent, while the southern nucleus NGC 4039 appears faint and shows a diffuse elongation towards southwest which is also found on the CO maps of Stanford et al. (1990). At 450 μm K1 and the northern nucleus are clearly seen, but the southern nucleus and K2 are dim. At the low flux level only an upper limit for K2 can be derived.

On the ISOPHOT maps two emission maxima show up at 100 μm (Fig. 1d), centred on the northern nucleus and the overlap region. The southern nucleus is not seen, nor does it produce a significant wing in the map. At 60 μm (Fig. 1e) only one broad peak located on the overlap region rises above the extended emission. Thus, the overlap region contains dust which is even warmer than in the northern nucleus.

Comparing the SCUBA and ISOPHOT maps, the location of the FIR maximum appears at a first glance closer to K2 than to K1 (Fig. 1d). But this is the consequence of the ISOPHOT observing and mapping procedure, where for the oversampled maps the 46″ detector is scanning with steps of 15″ × 23″, while the Airy profile for the ISO 60 cm telescope has about 21″ and 32″ FWHM at 60 and 100 μm, respectively. Note that no deconvolution was applied to the ISOPHOT maps. Instead, in order to investigate whether in the overlap area the FIR emission originates preferentially from K2 or also considerably from K1, we make use of known maps which trace the location of dust (and ISM) at high spatial resolution. These are the ISOCAM 15 μm, SCUBA 450/850 μm and VLA 6 cm maps. Note that in all these maps K1 is of similar or higher brightness as K2, and also that, in particular at 15 μm and 6 cm, the brightness profile is strongly asymmetric with a peak near the southeastern border and an extended emission towards northwest. We take them as input maps and simulate the ISOPHOT observing and mapping procedure. The input maps were (1) convolved to the corresponding Airy size of the ISO telescope at 60 and 100 μm, respectively, then (2) scanned as did the ISOPHOT detector along PA=33° with 15″ × 23″ steps, then (3) from the scanned raster grid an output image with 15″ × 23″ pixel size was created and (4) interpolated to 1″ pixel size for better visualisation. The results of these simulations are shown in Fig. 1 (f-i). Firstly, for all four input images the location of the maximum of the output image shifts about 10-20″ towards northwest, with an example shown in Fig. 1f. This shift can be understood as a consequence of sampling an asymmetric input brightness distribution with a peak near the southeastern border. Thus, the true 60 and 100 μm maximum could lie towards southeast of the apparent location in the observed ISOPHOT images. Secondly, the observed images coincide well with the simulations (Fig. 1g-i). This suggests that the FIR emission, in fact, originates also considerably from K1, and not only from K2 (or northwest of it), as was the impression at the first glance (Fig. 1d-e). Furthermore, the 6 cm and 15 μm input maps result in simulated peaks encompassing the observed one at 60 μm (Fig. 1g-h). Thus, the brightness ratio R between K1 and K2 at 6 cm (R ≈ 0.7) and at 15 μm (R ≈ 2.3) may provide limits for a tentative estimate of the K1/K2 ratio at 60 μm; the mean of about R ≈ 1.5 argues in favor of K1 being slightly brighter at 60 μm than K2. This is also well consistent with K1 being brighter than K2 at 450 μm. At 100 μm (Fig. 1i) the observed broad maximum in the overlap region is excellently reproduced by the simulation with the 850 μm input map. Furthermore, compared to K1 + K2 the northern nucleus appears fainter at 850 μm than at 100 μm, indicating that the overlap region contains a stronger cold dust component (besides the warm one mentioned above).

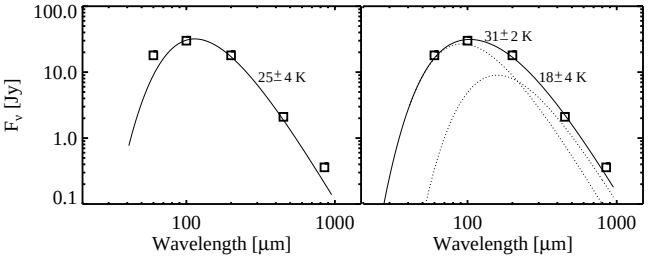

Fig. 2. SED of the two submm knots in the overlap area (sum of K1 and K2). The errors are within the size of the squares. The FIR fluxes at 60, 100 and 200 μm are 30% of those of the total galaxy listed by Klaas et al. (1997). This fraction is justified by the simulations described in the text. Fits with one modified blackbody *(left)*, and two modified blackbodies *(right)*, each with emissivity λ^{-2}. The temperature errors were determined by fitting the steepened and flattened flux constellation with 30% higher/diminuished FIR flux, respectively.

The ISOPHOT maps are consistent with KAO maps presented by Evans et al. (1997) at 60 μm, and by Bushouse et al. (1998) at 100 and 160 μm. Similarly the KAO maps are oversampled using a detector pixel size of about 45″, thus they likely suffer also from the convolution and show the observational shift of the flux maximum pointed out by our simulations.

Spectral analysis: At 15 μm and 6 cm the knots K1 + K2 together comprise about 30-35% of the total flux (within 2′ diameter). Assuming for the knots a similar contribution also at 60, 100 and 200 μm and taking the FIR flux values from Klaas et al. (1997), the FIR to submm spectral energy distribution (SED) can be derived for K1 + K2 (Fig. 2). A single modified blackbody fit of the 100 to 450 μm data with T = 25 K (which is unusually cool for an active starburst galaxy) yields a remaining flux excess at both 60 and 850 μm. This suggests the presence of dust components which are both warmer and colder than 25 K, respectively. A better fit to the SED is obtained with two modified blackbodies, one with T = 31 K (which is more typical for starburst galaxies) and one with T = 18 K (which is again rather cold). The presence of the 18 K component in the overall

Table 1. Properties of the submm knots: Fluxes are within 30″ apertures, with 1-σ errors about 0.3 Jy at 450 and 0.02 Jy at 850 μm. The formal colour temperature $T_{450/850\,\mu m}$ and L are derived from modified blackbodies with emissivity λ^{-2}. The temperature errors were determined by fitting the steepened and flattened extreme constellations with 0.5 sigma added/subtracted to the measured fluxes. M is calculated according to Hildebrand (1983).

Obj	RA J_{2000}	DEC J_{2000}	450 μm [Jy]	850 μm [Jy]	T [K]	L 10^9 [$L_\odot$]	M 10^7 [$M_\odot$]
Nuc4038	12:01:52.9	-18:52:05	1.69	0.25	16^{+6}_{-3}	1.9	2.8
Nuc4039	12:01:53.2	-18:53:08	1.06	0.15	16^{+6}_{-3}	1.2	1.7
K1	12:01:54.9	-18:53:02	1.33	0.19	16^{+6}_{-4}	1.5	2.2
K2	12:01:55.2	-18:52:47	$4\sigma = 1.20$	0.17	$<15^{+2}_{-6}$	<1.0	>2.2
			$3\sigma = 0.90$		$<11^{+4}_{-2}$	<0.3	>3.8

spectrum of K1 + K2 is consistent with the 450/850 μm colour temperatures derived for the single knots. Table 1 lists for all four knots the submm fluxes and derived parameters. Depending on the choice of the 450 μm upper limits for K2, the temperature reaches extremely cold values down to about 11 K, like found for protostellar condensations. The 450 μm data, however, are rather noisy and the difference between K1 and K2 should be considered with some care – we discuss it further below together with other observational results.

The radio 6 and 20 cm continuum (Hummel & van der Hulst 1986) extrapolated to 850 μm is very faint (< 10 mJy) and its contribution in the submm range can be neglected. On the other hand, high excitation CO lines are found in warm regions of starburst galaxies (e.g. Wild et al. 1992, Devereux et al. 1994). Thus, in our Arp244 maps the broad band 850 μm filter could contain also flux from the CO 3-2 line at 870 μm with an excitation temperature $T > 30$ K. In this case the 450/850 μm colour temperature would be warmer and the dust mass lower than listed in Table 1. But as seen in Fig. 2 (right), the observed 850 μm flux lies clearly above the blackbody curves, allowing for a CO 3-2 line flux of $F_{max} \approx 120$ mJy, i.e. 30% of the 850 μm flux. This is well consistent with the spectral line contributions of 28% to the SCUBA 850 μm fluxes derived by Johnstone & Bally (1999) for the Orion A cloud which contains the nearest site of ongoing high mass star formation. Currently, for Arp244 no published CO 3-2 line fluxes are available, so we try some further estimates: F_{max} is also compatible with the estimates ranging from 40 to 56 mJy derived for the CO 3-2 flux of K1+K2 by scaling the measured flux F (CO 1-0) with typical ratios R = CO 3-2 / CO 1-0 for starburst galaxies. We used $F_{K1+K2} = 225$ Jy km s^{-1} measured by Stanford et al. (1990, their Table 1, with a spectral resolution r = 13 km s^{-1} and a line width / bandpass ratio CO 3-2 / 850 μm filter $\approx 3.6 \cdot 10^{-3}$) and the average ratio R = 0.64 ± 0.06 obtained for nuclear starburst regions by Devereux et al. (1994, their Table 3) and R = 0.9 ± 0.2 for M 82 by Wild et al. (1992), respectively. F_{max} is even yet compatible for a three times higher CO 1-0 flux which was suggested by Nikola et al. (1998). Similarly, a possible CO 6-5 line contribution at 435 μm to the SCUBA 450 μm flux requires even higher excitation temperatures and might be too small to affect our dust temperature estimates (F (CO 6-5) < 100 mJy or < 5 %, derived with values from Stanford et al. 1990 and Wild et al. 1992). Thus, the 450/850 μm data are well consistent with a cold dust component at temperature of about 18 K or less.

4. Discussion

Off-nucleus dust concentrations: The observations impressively show that in this colliding galaxy pair the dust is accumulated not only in the two nuclei, but is also strongly concentrated in giant cloud complexes in the overlap region of the galaxy disks. At our spatial resolution the knots represent rather cloud complexes than single clouds (10″ $\approx$ 1 kpc). Furthermore, besides the relatively warm dust at T $\approx$ 30 K which is a characteristic temperature for starbursts in luminous IR galaxies, much of the dust is probably cold at $T < 20$ K which is more typical for quiet galaxies and extremely dense clouds. In the following we focus on knots in the overlap area only.

Nature of the knots: The two knots K1 and K2 in the overlap area show an excellent spatial coincidence with peaks seen on maps at 15 μm, CO 1-0 and 6 cm. We argue now that both knots show starbursts as well as quiescent regions.

The brightest 15 μm peak (#2) is located at K1. Thus, K1 contains already clouds well heated by the strong starbursts. K2, however, could still be mainly composed of clouds in a pre-starburst phase. Firstly, the flux of the 15 μm peaks coincident with K2 is about a factor of three fainter than for K1. If the star formation rate were actually higher in K2 than in K1, then also the extinction in the MIR must be higher for K2 than for K1, but K2 will outshine K1 somewhere in the FIR and submm domain. This, however, is neither indicated by our FIR data simulations, nor is it observed in the submm domain. The possibility, that K2 suffers still from extinction at 450 μm, is very unlikely. K2's opacity can be derived from the dust mass where we adopt that a dust column density of 0.1 $M_\odot$ corresponds to an optical depth of $\tau_V \approx 0.5$. For example, distributing a dust mass of 10^7 $M_\odot$ homogeneously within a slab of 300 pc radius (3″) yields $\tau_V \approx 170$, or following Mathis et al. (1983, their Table C1) $\tau_{450\,\mu m} \approx 0.1$, hence negligible. Secondly, the 450/850 μm flux ratios indicate for K2 rather a lower temperature and luminosity than for K1, suggesting that in K2 starbursts are spatially confined or moderate or too young to have yet heated the bulk of the dust like in K1.

Stanford et al. (1990) already suggested from the lack of H_α emission in the area around K2 that, if star formation took place, then it would be totally obscured. Their 6″ resolution CO maps show, besides the two nuclei, also very prominent emission in the overlap region which is resolved into four peaks. The brightest one in the south coincides with the warm knot K1, while the three much fainter ones (E,W and N in Stanford et al.'s notation) are located at the position of the cold knot K2. Thus, K2 appears to be clearly resolved into smaller units on the CO maps. Notably the CO emission of K2 is about 50% of that for K1 (Stanford et al. 1990), but new CO maps with the BIMA array show a more equal CO brightness for K1 and K2

(Gruendl et al. 1998, Gao et al. 1998). Nikola et al. (1998) derived a low flux ratio CII 158 μm line / CO for the whole galaxy and concluded that the active regions might be surrounded by quiescent ones. These could just be the cold regions like we see in K2 (and also in K1).

VLA 6 and 20 cm radio continuum maps also show – besides the two nuclei – a couple of prominent peaks in the overlap region (Hummel & van der Hulst 1986). Their peak #2 lies in K1, and their peaks #3 and #4 in K2. At 20 cm peak #3 in K2 is by far the brightest one and has the steepest spectral index ($\alpha_{6/20\,\mathrm{cm}} \approx$ -0.6 $\pm$ 0.2) among the other peaks ($\alpha_{6/20\,\mathrm{cm}} \approx$ -0.4 $\pm$ 0.2). While K2 is less luminous and shows less signatures for starburst activity compared with K1, the 20 cm radio continuum in K2 is brighter and has a steeper spectrum than that in K1. Therefore, the strong radio continuum could be due to small clusters of compact HII regions and supernova remnants which are hidden on the back side of the dust clouds. They are invisible at optical wavelengths and possibly suffer strong extinction in the mid-infrared, and they belong to the first generation of starbursts, so that the bulk of the dust has not yet been heated substantially. An alternative explanation is, that in K2 the strong radio continuum is the consequence of an enhanced magnetic field still compressed within the dense clouds. Then a modest star formation or shocks in the interstellar medium are sufficient to provide the electrons for the strong synchrotron emission. Note, that in a turbulent environment like K1 and K2 only little is known about the validity of the radio-FIR correlation and that magnetic field strength needs not to be in equipartition with the cosmic rays or star formation rate. If K1 is more evolved than K2, then any compression of the magnetic fields could already be relaxed in K1 and less radio continuum would be seen. Future polarimetric radio observations should provide clues to this puzzle.

In conclusion, besides the strong starburst activities in particular in K1, many of the dust clouds in K1 and K2 are cold. K2 shows the lower dust temperature and luminosity and also lower or younger starburst activity, but the strongest radio peaks at 6 and 20 cm. This suggests that, in addition to the starbursts, exceptional conditions are present. They are consistent with the picture of an extreme compression of the ISM in clouds, in which case these clouds could be in a pre-starburst phase housing many protostellar condensations.

Genesis of the knots: From the morphology we sketch the following evolutionary scenario: The separation of K1 and K2 is about 2 kpc (20″). The overlap region contains about 10^7 $M_\odot$ dust which comprises a considerable fraction (10-30%) of the typical dust content of a whole spiral galaxy. Such a concentration within a projected size of 1-3 kpc could be explained as a consequence of an initial inelastic collision of clouds of the two galaxy disks which serves as a kernel into which the other clouds of the rotating disks are running – like a traffic jam in the fog.

The life time of molecular clouds in the Milky Way is less then 10^7 years and probably much shorter in turbulent environments (A. Burkert, private communication). Taking a typical maximum sound speed of 10-100 km/s for the dust clouds, the dynamical time scale to cross the distance between K1 and K2 is about 10^8 to 10^9 years or longer. This clearly exceeds the 10^6 to 10^7 years lifetime of the clouds in K1 and K2 as well as that of the OB stars generated in K1. Thus the knot K2 can not be triggered by K1, rather it was independently created.

Generalisation to mergers: While the bulk of the dust in Sb and Sc galaxies has a temperature of about 15-20 K (e.g. Chini et al. 1986), dust in mergers and active galaxies was believed to be warmer, with most of their FIR-submm luminosity coming from dust at T $>$ 30 K (Chini et al. 1989). The spatially resolved observations of Arp244, however, suggest that mergers of dusty galaxies in general contain dense concentrations of cold dust at T $<$ 20 K as well.

Acknowledgements. It is a pleasure for us to thank Rainer Beck (MPIfR, Bonn) for stimulating discussions and for providing the VLA 6 cm radio map, and and Olivier Laurent (CEA, Saclay) for the ISOCAM 15 μm and HST V band maps. We also thank Andreas Burkert for valuable discussions, and Stefan Hotzel and Linda Schmidtobreick (MPIA) for support in creating the overlays. JCMT is operated by the Joint Astronomy Centre on behalf of the Particle Physics and Astronomy Research Council of the United Kingdom, the Netherlands Organisation for Scientific Research, and the National Research council of Canada. ISO is an ESA project with instruments funded by ESA Member States (especially France, Germany, the Netherlands and the United Kingdom) and with the participation of ISAS and NASA. The development and operation of ISOPHOT and the Postoperation Phase are supported by MPIA and funds from Deutsches Zentrum für Luft- und Raumfahrt (DLR, formerly DARA). The Interactive Analysis tool PIA is a joint development by the ESA Astrophysics Division and the ISOPHOT consortium. We thank the referee Anne Sansom for helpful comments.

References

Bushouse, H.A., Telesco, C.M., Werner, M.W., 1998, AJ 115, 938
Chini R., Kreysa E., Krügel E., Mezger P.G. 1986, A&A 166, L8
Chini R., Krügel E., Kreysa E., Gemünd H.-P. 1989, A&A 216, L5
Devereux N., Taniguchi Y., Sanders D.B., et al., 1994 AJ 107, 2006
Evans R., Harper A., Helou G., 1997, in "Extragalactic Astronomy in the Infrared", p. 143, Eds. G.A. Mamon, T.X. Thuan and J.T.T. Van. Paris: Editions Frontieres
Gao Y., Gruendl R.A., Lo K.Y., et al. 1998, AAS, 192, #69.04
Gruendl R.A., Gao Y., Lo K.Y., et al. 1998, AAS, 192, #69.05
Hildebrand R.H. 1983, Quart. J. Royal. Astron. Soc. 24, 267
Holland W.S., Robson E.I., Gear W.K., et al., 1999, MNRAS 303, 659
Hummel E., van der Hulst J.M., 1986, A&A 155, 151
Johnstone D., Bally J., 1999, ApJ 510, L49
Kessler M.F., Steinz J.A., Anderegg M.E., et al., 1996, A&A 315, L27
Klaas U., Haas M., Heinrichsen I., Schulz B. 1997, A&A 325, L21
Lemke D., Klaas U., Abolins J., et al., 1996, A&A 315, L64
Mathis J.S., Mezger P.G., Panagia N. 1983, A&A 128, 212
Mirabel I.F., Vigroux L., Charmandaris V. et al., 1998, A&A 333, L1
Nikola T., Genzel R., Herrmann F. et al., 1998, ApJ 504, 749
Stanford S.A., Sargent A.I., Sanders D.B. et al., 1990, ApJ 349, 492
Whitmore B., Schweizer F., 1995, AJ 109, 960
Wild W., Harris A.I., Eckart A. et al., 1992, A&A 265, 447